Monomer Transport Influences in the Nascent Polymerization of Ethylene by Silica-Supported Chromium Oxide Catalyst

Steven W. Webb, W. Curtis Conner, and Robert L. Laurence*

Department of Chemical Engineering, University of Massachusetts, Amherst, Massachusetts 01003. *Received September 19, 1988; Revised Manuscript Received December 20, 1988*

ABSTRACT: Transport influences during nascent ethylene polymerization over Phillips chromium oxide–silica catalyst were evaluated by using pulse solid–gas chromatography. Measures of effective intraparticle diffusivity and tracer-accessible intraparticle void space were made using helium as a tracer. Measures of surface reaction rate and equilibrium adsorption were made using ethylene monomer as the tracer. Quantitative site poisoning using oxygen was performed. The Kubin–Kucera model was used for the transport measurements; the Suzuki–Smith model was used for the kinetic analysis. The Thiele modulus for ethylene polymerization at 50 °C, 1 atm of monomer pressure, and yields less than 0.1 g of polymer/g of catalyst is estimated to be 1.5. This value increases as polymer is formed inside the catalyst pores. Significant intraparticle concentration gradients and transport control may exist even at low yields. Without particle fracture, the rate of polymerization, which would occur mainly at the particle surface, would be inhibited. The rate of adsorption of monomer over active chromium oxide is very fast relative to the surface reaction. The apparent first-order polymerization rate constant at these conditions is roughly 0.06 s^{-1}. The estimated activation energy for the surface insertion step is 14 kcal/mol. The equilibrium adsorption constant is 6; the free energy for reversible adsorption is −3 kcal/mol. The effective intraparticle monomer diffusivity prior to particle fragmentation and accumulation of polymer is 2.5×10^{-4} cm^2/s, a very low value when compared to that estimated by using effective medium transport theory.

Introduction

The nascent period of the polymerization of ethylene from the gas phase by porous catalysts is a very important part of the overall polymerization. The morphology of the polymer particle obtained after polymerization to high yields is determined to a large extent by how the polymer is first incorporated into the high-porosity polymerization catalyst during nascent polymerization. Unlike the kinetics at high yields, the kinetics of nascent polymerization may be highly influenced by diffusion. The resistance to diffusion is due to the microporous and tortuous nature of the transport path through the catalyst macroparticle and the very high intrinsic activity of the catalyst at the outset of the polymerization. The limitation due to diffusion combined with a rapidly changing catalyst morphology and fast deactivation kinetics can lead to a highly unstable initial rate of polymerization. This instability in rate is difficult to control and can result in particle overheating. A temperature excursion in the polymerizing particle may lead to particle melting, agglomeration of particles, and possibly premature decay in the rate of polymerization.

It is important to study the nascent polymerization to determine means to prevent or reduce the instability in rate and to allow control of the polymer particle morphology. The kinetics may be influenced by diffusion so that the study should include measurements of both apparent rates of polymerization and transport. However, since the morphology and specific site kinetics change dramatically during the nascent polymerization, an empirical approach that does not account for the changes in the catalyst particle will not be successful. Here, we examine three aspects of the nascent polymerization kinetics of ethylene over chromium oxide catalysts: (1) the apparent adsorption and site insertion kinetics; (2) the influence of monomer diffusion and catalyst morphology; (3) the influence of catalyst activation and polymer accumulation.

The importance of monomer transport on the early kinetics has been considered in the models of Chiovetta and Laurence[1] and Ray et al.[2-4] These efforts were intended to provide insight into the influence of transport on the kinetics of the polymerization and on the instability of the initial rate of polymerization. In all these studies, the monomer diffusivity was estimated by using correlations from the literature. In fact, no measured monomer diffusivities for chromium oxide polymerization catalysts have been published. The phenomenon of particle fragmentation and its influence on the diffusion-limited kinetics were treated in a very simple manner.

The influence of activation of these catalysts on the particle morphology was studied by Weist et al.[5] using porosimetry. They found significant alterations of the catalyst micropore size distribution due to the oxidation and reduction steps during activation and polymerization. The influence of these morphological changes on polymerization kinetics was considered in the experimental studies of Ali,[6] Naik,[7] Weist,[8] and McDaniel[9] and have been reviewed by McDaniel[10] and Karol.[11] These studies concluded that high catalyst porosity is required to achieve high activity and activity longevity. They found that catalyst macroparticle fragmentation must occur at low yields to reduce the transport influence on the rate of polymerization. If fragmentation did not occur, ultimate yield of polymer was limited. In the absence of particle fracture and subdivision, pores will fill completely and polymerization will occur only at the macroparticle surface. Surface polymerization results in low and decaying rate of polymerization, particle agglomeration, and reduced ultimate yield. Further, Munoz-Escalona et al.[12] have shown that surface polymerization produces hollow, low bulk density polymer particles.

We use solid–gas chromatography (SGC) to measure both monomer diffusivity and the kinetics of ethylene polymerization. A model first developed by Kubin[13] and Kucera[14] is used in the analysis of the inert-gas pulse tracer response across a column packed with polymerization catalyst. This experiment provides estimates of tracer-accessible intraparticle void space and diffusivity. An extension of the Kubin–Kucera model, developed by Suzuki and Smith,[15] is used in the analysis of the pulse response of monomer injected across a column of catalyst. The Suzuki–Smith model reduces to the Kubin–Kucera model when there are no irreversible surface reactions.

* To whom all correspondence should be addressed.

0024-9297/89/2222-2885$01.50/0

This experiment provides estimates of adsorption, surface reaction, and adsorption equilibrium constants. Our experiments are performed on inactive catalyst, active catalyst, and partially polymerized catalyst. Thus, with a very simple experiment, insight into the nascent kinetics of ethylene polymerization over chromium oxide is obtained. We believe this may be the first use of this analysis and experimental method to estimate kinetic and transport properties of polymerization catalysts.

Theoretical Section

Quantitative solid–gas chromatography is reviewed by Conder and Young[16] and Furasawa.[17] Solid–gas chromatography has been used extensively to study solid–gas heat transport by Sagara,[18] chemisorption kinetics by Suzuki,[19] Padberg,[20] and Schneider,[21] irreversible or slow adsorption kinetics by Chui,[22] Galan,[23] and Cerro,[24] axial diffusion in packed columns by Edwards and Richardson,[25] Schanel and Schneider,[26] and Scott et al.,[27] intraparticle diffusivity in catalyst pellets by Baiker[28] and Cerro et al.[29] and in compressed zeolites by Sarma and Haynes,[30] and surface diffusion by Schneider.[31] Nonideal influences have been studied such as intraparticle convection by Nir and Pismen[32] and Rodrigues et al.[33] and nonisobaric operation by Dixon et al.[34] and Carleton and Kershenbaum.[35,36] Chromatography has been used to measure pore sizes directly by using a pore transport model proposed by Schneider and co-workers.[37] SGC has also been used to test models of pore morphology (Foth et al.[38]). The theory is well-developed, and tractable models can be used to evaluate equilibrium constants and transport rates in a simple and straightforward experiment.

The essential physics of SGC lies in the retention and broadening of a well-characterized pulse input of a tracer to a packed column of particles. As solute molecules travel along the column, they are retained by diffusion into and out of the pores of the catalyst particles, by chemisorption to the surface, by diffusion into boundary layers, and by axial dispersion. Only axial dispersion is dependent on carrier velocity, and its influence can be separated independently. At higher carrier flow rates, the influence of axial dispersion is diminished. By selection of a suitable operating region and pulse tracer gas, it is possible to eliminate all but the intraparticle influence.

The governing differential transport equations and solution method were developed originally by Kubin and Kucera[13,14] and later by Suzuki and Smith,[15] Miller and Bailey,[39] and Schneider.[40] The solution in the time domain is not feasible. A Laplace solution is used to represent the measurable dynamic properties of the elution curve as a function of the mass transport rate and volumetric properties of the packed column. The moments provide equations for the mean retention time and variance of the eluting peak, at a given carrier velocity, with a known pulse input of tracer.

The zeroth moment (peak area) represents the amount of eluting solute. The first moment (mean retention time) depends upon equilibrium or steady-state properties of the packing including equilibrium adsorption, solubility, and intraparticle volume. The second moment (variance) contains mass transport information including boundary layer dispersion, rate of adsorption, axial dispersion, and intraparticle diffusion. System contributions to the dynamics of the elution curve must be accounted for in the moment evaluation. These will include dead volume and dead time on the first moment and solute dispersion in fittings, flow lines, injector, and detector compartments. Finally, the influence of pressure drop must be accounted for in the analysis.

Evaluation of total porosity involves plotting the mean retention time (μ_1) with inverse carrier velocity (v_∞), as shown in eq 2. For isobaric conditions, the line will be linear with a zero intercept. The slope of the line indicates total porosity, which includes both column free space (α) and intraparticle pore volume (β). The intercept of the line will be nonzero if there is a pressure drop in the column. Evaluation of transport rate parameters requires plotting the variance (s^2) of the elution curves with inverse carrier-gas velocity squared, as shown in eq 3. Again, for isobaric operation this line will be linear. The slope of the line produces an estimate of axial diffusivity; the intercept gives an estimate of intraparticle diffusivity. Curvature, especially noticeable at higher carrier flow rates, is indicative of a significant pressure drop and should be avoided to preserve linearity in the analysis.

$$\mu_0 = 1 \tag{1}$$

$$\mu_1 = (L/v_\infty)[\alpha + (1-\alpha)\beta] \tag{2}$$

$$\frac{s^2}{2(L/v_\infty)} = \frac{(1-\alpha)}{15}\beta^2\frac{R^2}{D_{\text{eff}}} + D_{\text{L}}\alpha^2\left\{1 + \frac{(1-\alpha)\beta}{\alpha}\right\}^2\frac{1}{v_\infty{}^2} \tag{3}$$

Considering the case of a reacting tracer (i.e., ethylene over active catalyst) the analysis has been worked out by Suzuki and Smith.[15] For the simplified case in which column conditions are chosen such that axial diffusion and external film diffusion transport are negligible, eq 4–7 are used to describe the moments of the monomer elution curve. Note that eq 5 defines the Thiele modulus for the reaction.

$$\mu_0 = \exp\left\{-\frac{\alpha(L/v_\infty)}{R^2/D_{\text{eff}}}\,\frac{(1-\alpha)}{\alpha}\phi^2\right\} \tag{4}$$

$$\phi^2 = \frac{\beta R^2}{D_{\text{eff}}\left\{\dfrac{1}{k_{\text{ads}}} + \dfrac{1}{k_{\text{rxn}}}\right\}} \tag{5}$$

$$\mu_1 = \frac{L}{v_\infty}\left\{\alpha + (1-\alpha)\beta\left(1 + \frac{\phi^4}{\beta^2(R^2/D_{\text{eff}})^2 k_{\text{rxn}}{}^2 K_{\text{A}}}\right)\right\} \tag{6}$$

$$\frac{s^2}{2(L/v_\infty)} = \frac{(1-\alpha)}{15}\beta^2\frac{R^2}{D_{\text{eff}}}\left\{1 + \frac{\phi^4}{\beta^2(R^2/D_{\text{eff}})^2 k_{\text{rxn}}{}^2 K_{\text{A}}}\right\}^2 + \frac{(1-\alpha)\beta\phi^6}{\beta^2(R^2/D_{\text{eff}})^3 k_{\text{ads}} k_{\text{rxn}}{}^3 K_{\text{A}}} \tag{7}$$

A Fourier domain solution and Fourier fitting (Gangwal,[41] Pawlisch[42]) is sometimes preferable in quantitative chromatography especially with strongly adsorptive solutes or in applications where base lines tend to drift during the solute residence time. This is frequently the case with solute–polymer transport. However, in this work, Fourier analysis was not required. Since the time scale of the elution is quite small and desorption processes are fast, base lines were exceptionally stable. In cases where the number of data points is limited, smoothing of the data prior to moment calculations is required.

It is important to recognize that SGC is an unsteady-state experiment and will yield an unsteady-state diffusion coefficient. SGC is sensitive to only those rate processes or dynamic equilibria that occur much faster than the average solute residence time in the column. Severe complications in the analysis result if a slow rate process is being measured (Chui,[22] Galan[23]). Thus, transport prop-

erties measured in an SGC experiment will not necessarily correspond to those measured in a steady state or equilibrium experiment.

Baiker et al.[28] have evaluated the difference between those estimates of diffusivity in a steady-state experiment (Wicke–Kallenbach method) and SGC. This work, done on a set of commercial catalyst pellets, led to the conclusion that there was no significant difference between the two techniques. Cerro and Smith[29] reported one difficulty of SGC with nonadsorptive tracers to measure intraparticle diffusivity. They found that accurate and careful correction for system effects was essential, since system influences were a significant part of the pulse dispersion dynamics.

Kinetics of polymerization have never been studied in a pulse SGC experiment. In fact, obtaining kinetic information from an SGC pulse experiment is nontrivial. Earlier studies by Kokes,[43] Gaziev,[44] Blanton,[45] Wetherold,[46] and Cho and Aris[47] demonstrated the difficult problem of estimating kinetic parameters with reactant concentration variation in both time and space. Groeneveld et al.[48] did ethylene polymerization in a packed column but did not use an analytical model to retrieve reaction rate constants. They performed step monomer concentration injections and observed severe nonisothermality. They used a low-porosity chromium oxide catalyst and claimed that all polymerization occurred at the surface of the particle.

In the present work, we use pulse monomer feeds to ensure isothermal operation. The Suzuki and Smith model provides values of adsorption equilibrium constant, adsorption rate constant, and reaction rate constant. The first three moments of the monomer elution peak under reaction conditions are required. It is necessary to operate at the highest, isobaric, carrier velocity to minimize the influence of axial and boundary layer dispersion. The only rate parameter that must be independently fixed is intraparticle diffusivity. This parameter is obtained from the Kubin–Kucera analysis with the diffusivity estimate corrected for the molecular weight difference between the tracer gas and monomer.

Experimental Section

The experimental apparatus is similar to that used by Schneider and Smith.[21] A quartz glass column, 36 cm long and 4 mm in diameter (4.61 cm^3) was packed by vigorous mechanical vibration with approximately 1.2 g of sieved polymerization catalyst. The catalyst used was supplied by Phillips Petroleum. The catalyst comprised nominal 0.9% chromium on Davison 952 silica of pore volume 1.7 cm^3/g (79% porosity). The catalyst was characterized by mercury porosimetry (Weist et al.[5]). Roughly half of the internal void space is contained in micropores (pores of dimension less than 50 Å); the balance being in macropores (pores of dimension greater than 200 Å).

The experimental apparatus is shown in Figure 1. The carrier gas was nitrogen, at flow rates from 10 to 30 cm^3/min with superficial velocities of 1.0–4.0 cm/s and retention times of 10–50 s. Carrier flow was measured with a bubble flow meter and adjusted with a needle valve. The carrier gas flowed through a molecular sieve to remove oxygen and water. Tracer gas was ultrahigh-purity helium, injected from a 0.25-cm^3 gas sample loop at 75 °C and 19 psig. A separate gas system for carbon monoxide and oxygen was used to perform the catalyst activation by sequential oxidation and reduction. All carrier lines after the sample loop were 0.010-in. i.d. tubing to minimize dead volume. A Hewlett-Packard 5880 gas chromatograph was used, with a TC detector.

Column volume was measured by the pulse response of an empty column, by using the same method and procedures as with packed columns. System dispersion, dead time, and dead volume were evaluated over the flow-rate range used by removing the column and replacing it by a zero dead-volume union. Pressure drop was evaluated at a range of flow rates. Column head pressure (before injector) was 3–5 psi above atmospheric; column outlet was to the atmosphere. No correction for carrier compressibility was made, and carrier velocity was assumed to be uniform.

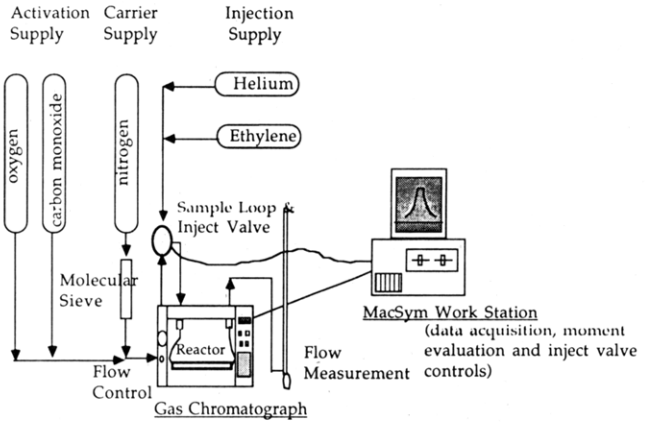

Figure 1. Solid–gas chromatography experimental apparatus.

Data were collected by an Analog Devices computer at 0.05-s sampling interval. Moments were evaluated with a minimum of 300 points for each elution curve so that no filtering or smoothing of the peaks was used. Measured moments were corrected for the system influences described above. The mean retention time was linearly regressed with inverse carrier-gas flow rate (expressed as column volume divided by carrier flow rate) to evaluate total porosity changes. The variance was linearly regressed with inverse carrier velocity squared. A minimum of 15 injections was used to do the regression, including replicates. Column external porosity was calculated from the known pore volume (from porosimetry), solid density, and column volume.

Catalyst solids were dried in nitrogen at 150 °C for 2–4 h in flowing nitrogen. Tracer testing was then done with helium. The catalyst column was then removed, without detaching the flow lines or interrupting carrier flow, to an adjacent tube furnace. The catalyst was then calcined in flowing oxygen at 770–820 °C for 3 h. After calcination, the catalyst is a bright orange color. After cooling in oxygen, the column was replaced in the GC oven, again without detaching the flow lines or interrupting carrier flow, and tested again for morphological changes. Finally, the catalyst was reduced with carbon monoxide for 1 h at 300 °C and again tested with tracer injections. After reduction, the catalyst is a light blue color and is ready for polymerization. In the analysis, it is necessary to assume that no change in catalyst particle size occurred due to calcination. All changes in solute elution curves are then due to internal alterations of the catalyst morphology.

Since it was not possible to contain the entire column with solids in the furnace for calcination (without melting the end ferrules), some catalyst remained unactivated at each end. Oxygen and water are severe catalyst poisons, and great efforts were made to ensure leakproof operation and pure feed gases to the column. Verification of the potential activity of the catalyst was possible by viewing its color change after each activation step. Catalyst poisoning was done by injecting measured quantities of oxygen through the gas sample loop into the live catalyst column. Polymerization was done by injecting 2-cm^3 pulses of ethylene monomer (polymerization grade) at 20 psi and 75 °C over the live catalyst. A larger injection volume was required to provide a measureable elution area (since ethylene is being consumed). Upon treatment with monomer, the catalyst would become a darker blue. After sufficient polymerization, it would become white, due to the presence of polyethylene.

Results and Discussion

Preliminary Testing of Dry Solids: Verification of SGC. Solids tested were nonporous glass beads with an average particle size of 180 μm, an α-alumina of average size of 750 μm and 0.27 cm^3/g pore volume, and the polymerization catalyst of average size 187 μm (dry sieved fraction between 125 and 250 μm) and 1.7 cm^3/g pore volume. The glass beads were used to verify the technique,

Table I
Solute Diffusivity and Accessible Void Space of Tested Solids with Helium as a Tracer at 50 °C and 1 atm of Pressure[a]

solid	extraparticle porosity (α)	intraparticle porosity (β, SGC)	intraparticle porosity (β, porosimetry)	intraparticle diffusion time (R^2/D_{eff}), s	intraparticle diffusivity (D_{eff}), 10^{-4} cm^2/s	axial diffusivity (D_L), cm^2/s
none	1.000	0.0	0.0	0.0	0.0	0.948 (0.022)
glass beads	0.383	0.0	0.0	0.00.0	0.0	0.418 (0.139)
alumina	0.336	0.512 (0.019)	0.539	0.126 (0.040)	443 (160)	0.521 (0.040)
catalyst	0.415	0.667 (0.020)	0.789	1.580 (0.090)	2.41 (.12)	0.343 (0.040)

[a] Estimated precision of estimates in parentheses.

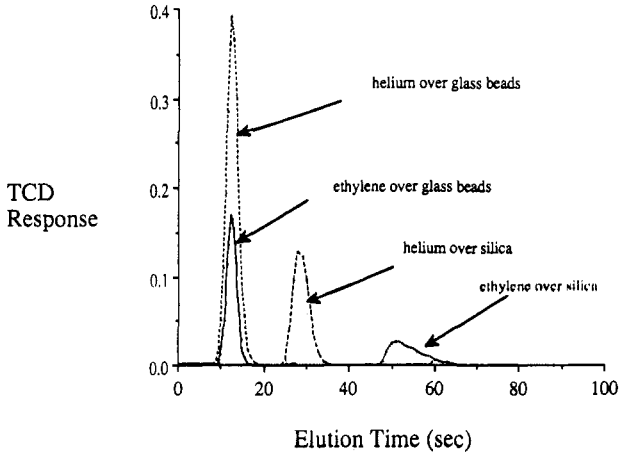

Figure 2. Influence of adsorption and intraparticle void space on the elution of helium and ethylene tracers at 50 °C (all at the same carrier flow rate).

to provide a standard to track system pressure drop and dynamics, and to evaluate boundary layer effects for 180-μm particles.

Figure 2 shows elution curves for helium and ethylene, with the nonporous glass beads and catalyst at the same carrier flow rate and temperature. The shape of the elution curves for noninteracting tracers was symmetric; the shape with interacting tracers was skewed. The influence of internal void space is significant both in increasing retention and elution curve variance. The influence of adsorption is much more pronounced. Example moment plots are shown in Figures 3 and 4. System effects were about 10–20% of the measured moments, and diligent accounting for these influences was required. Linearity of all experiments with either first or second moment plots was observed. Particle Reynolds number is calculated as 0.03.

Carleton et al.[35] have shown that a finite nonzero first moment intercept at the ordinate is indicative of a small column pressure drop. Their analysis shows that the slope of the first moment plot with a small pressure drop is independent of pressure drop. This is fortunate since the model nonlinearity that would be necessary to compensate for axial variation in solute concentration, axial diffusivity, and velocity due to pressure variation is not required. The intercept at the ordinate contains information about the pressure drop in the column and is of no consequence in the analysis.

Characteristic second moment plots are found in Figure 4. The influence of pressure drop on the second moment followed closely the results of Kershenbaum.[36] Curvature in the variance plot was found for carrier velocities is excess of 3 cm/s at column conditions. We restrict second moment analyses only to the linear portion of the variance plot to keep the analysis simple.

The second moment for the system is found to be independent of gas velocity. This would suggest that

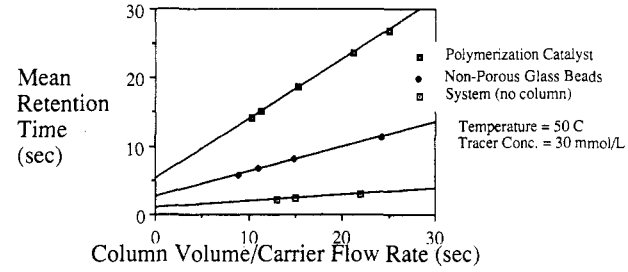

Figure 3. First moment of helium elution peak at 50 °C and 1 atm for different column packings: (1) system without column; (2) nonporous glass beads; (3) porous polymerization catalyst.

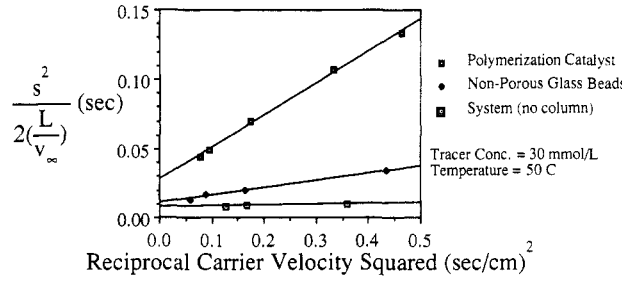

Figure 4. Second moment of helium elution peak at 50 °C and 1 atm for different column packings: (1) system without column; (2) nonporous glass beads; (3) porous polymerization catalyst.

mass-transfer effects, such as axial back-mixing and Taylor dispersion in carrier lines, detector, and injector, are insignificant. The injection of tracer may be characterized by a square wave of constant duration. The intercept for the glass beads is insignificantly different from the system effects, indicating that particle boundary layer and intraparticle dispersion are negligible at these carrier velocities and particle size. The second moment intercept for the catalyst is significant, demonstrating the influence of the porous internal structure in broadening the pulse input.

The results shown in Table I demonstrate that the measured internal void fraction (β) is consistently less than the calculated value from porosimetry. This implies that in the time frame of the elution, tracer does not penetrate all of the accessible void space. SGC will be sensitive only to that void space which is most easily accessed by solute, which will be mainly the macropores. Precision of the technique was found to be better than 2% based on replicate injections.

The axial diffusivity with an empty column is the estimated bulk molecular diffusivity of helium at column conditions, which compares with a value of 0.88 cm^2/s.[29] The value of diffusivity in alumina is consistent with effective medium theory (EMT), and one can calculate a value of tortuosity for this solid at around 10. Applying EMT to the polymerization catalyst, one gets a value of tortuosity at around 1500. This value is much too high to be credible and suggests that EMT may not be safely

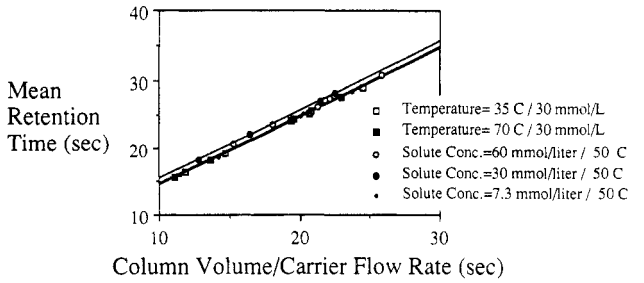

Figure 5. Influence of column temperature and solute concentration on mean retention time of helium tracer.

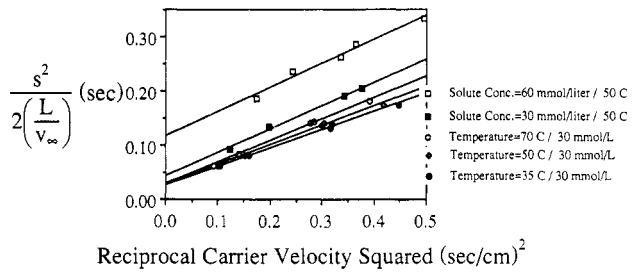

Figure 6. Influence of column temperature and solute concentration on elution peak variance of helium tracer.

applied to high-porosity solids in transient transport experiments. Note that since the average pore size of the polymerization catalyst is greater than the mean free path of helium at column conditions, a molecular diffusivity is used in the EMT calculation. However some pores of the solid are smaller than the mean free path and may have an exaggerated influence on the transport rate. Bulk column tortuosities may also be calculated and these were found to be in the range 0.9–1.1 and highly sensitive to column packing.

Since SGC is a transient technique, it is prudent to evaluate the sensitivity of its predictions with differing amounts of injected tracer and column temperature. These tests were done with dried polymerization catalyst. As shown in Figure 5, increasing column temperature and amount of injected solute results in very minor changes in the observed first moment. This confirms both the linearity of the experiment and the insensitivity of the first moment to all influences except void space and thus verifies the model of the experiment. In contrast to the first moment, the second moment or transport rate processes are very sensitive to experimental conditions. Figure 6 shows that increasing temperature increases elution curve variance, mostly due to increasing axial diffusion. Intraparticle diffusion appears to be temperature-insensitive across this narrow temperature range. Also shown in Figure 6, increasing the amount of tracer increases elution peak variance significantly. This effect is mainly due to a large decrease in the intraparticle transport rate. Axial diffusion is insensitive to pulse concentration. Note that pulse concentration is expressed as moles of helium injected per intraparticle pore volume.

These observations lead us to conclude that the results of an SGC experiment are highly sensitive to the dynamics and conditions of the particular experiment. It is doubtful that the values of void space or diffusivity are universally applicable. The results do describe the transport rate and apparent internal void space of the solid under the conditions of the experiment. Since there are no other values of effective diffusivity for polymerization catalysts in the literature, there is no basis for comparison.

The virtue of the experiment that is being exploited in this work is not that the predictions are accurate but that they are precise. This precision gives the technique the sensitivity to detect morphological changes due to activation and/or polymerization.

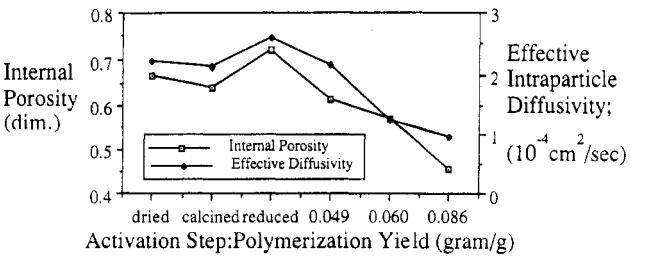

Figure 7. Effect of catalyst activation and nascent polymerization on apparent intraparticle accessible void space and tracer diffusivity.

Influence of Activation and Polymerization on the Morphology of the Polymerization Catalysts. The influence of the activation steps on the apparent void space and diffusivity is shown in Figure 7. Activation is a two-step process involving a high-temperature oxidation and subsequent reduction. The void structure of the polymerization catalyst is bimodal and comprises macropores (>200 Å) with 50% of the pore volume. Porosimetry results of Weist et al.[8] show that calcination causes an increase in total porosity. This increase is mainly in the micropore region. The macropore region shows a minor decrease in void volume. Catalyst reduction causes a drop in void space across all pore sizes.

SGC shows that apparent void space and diffusivity drop after calcination. This result is consistent with changes in the macropore region of the porosimetric results. The correlation between porosity and diffusivity is consistent with the EMT model. As macroporosity drops, so does diffusivity. SGC shows that subsequent catalyst reduction restores the accessible void volume (β) and diffusivity. This does not agree with the porosimetry which finds that all pore sizes decrease in volume. The overall influence of activation on diffusivity and apparent void space is minimal.

After activation the catalyst is exposed to monomer pulses. The creation of solid polymer inside the catalyst will alter the accessible void space and transport rate. To ensure that the measured void space alterations are internal, rather than external, the overall yield was kept low. Figure 7 shows the influence of polymerization to 0.1 g of polymer/g of catalyst yield on internal void space and solute transport rate. It is observed that internal void space and transport rate decrease significantly. Polymerization to such low yields fills the macropores of the catalyst nearest the external particle surface with polymer. This reduces accessible void space, slows monomer diffusion into the particle, and reduces solute penetration. At yields greater than 0.1 g of polymer/g of catalyst, large variations in retention time (first moment) and variance (second moment) and noticeable column shrinkage were observed. This was due to excessive polymerization on the surface of the particles, which caused interparticle fusion rendering the analysis, based on constant particle size and packing, invalid.

Ali[6] and Weist[8] studied the effect of polymer accumulation on the pore size distribution (PSD) of the polymerizing particle and catalyst macroparticle (after polymer removal) using mercury porosimetry. Polymerization was done at less than 1 atm of monomer pressure. They found that polymer accumulates initially mainly in macropores and reduces the void volume accessible to mercury considerably. These results are in general agreement with our observations using SGC.

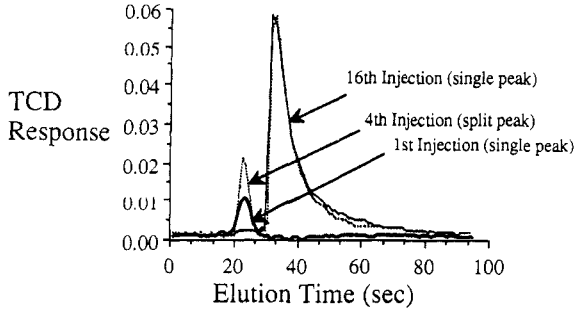

Figure 8. Transient adsorption of ethylene over freshly activated chromium oxide catalyst.

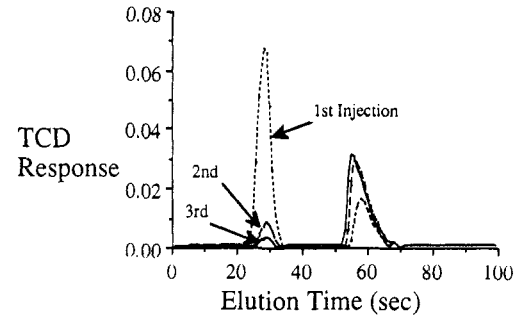

Figure 9. Transient adsorption of ethane over freshly activated chromium oxide catalyst.

Polymerization Kinetics with SGC. The rate of polymerization in homogeneous medium is commonly expressed as the following:

$$R_p = k_p[R][M] \tag{8}$$

where R_p is the rate of disappearance of monomer per unit reactor volume and unit time. In heterogeneous medium, the bulk-phase monomer concentration and available site concentration will differ by the amount of adsorption. The rate of polymerization in this case is given by

$$R_p = \frac{1}{\frac{1}{k_{ads}} + \frac{1}{k_{rxn}K_A}}\alpha[M] \tag{9}$$

where the kinetic parameters for adsorption from the bulk phase, surface reaction, and adsorption equilibrium are identified. When adsorption is very fast, relative to surface reaction, the expression becomes

$$R_p = k_{rxn}K_A\alpha[M] = \alpha[M]/\tau_{insertion} \tag{10}$$

where we define the insertion time constant, $\tau_{insertion}$. In our results to follow, we define the insertion rate constant as the inverse of the insertion time and the reaction rate constant as k_{rxn}. Both have units of inverse time. The insertion time contains kinetic information about the overall rate of polymerization or insertion of monomer. The rate constant, k_{rxn}, contains only kinetic information about the surface reaction step, independent of adsorption. We note that measured or average insertion time is directly proportional to the number of active sites and to the amount of monomer on the surface.

In the SGC experiment we can independently measure both k_{rxn} and K_A in a single elution at given conditions. The number of sites is implicitly included in these two parameters of the SGC analysis. Since the number of sites participating in sorption and reaction may not be the same, it is not possible to explicitly incorporate the site concentration in the rate expression. By poisoning the catalyst in a quantitative manner, we can extrapolate the estimated kinetic parameters and get an indication of the number of active sites participating in each process. Note that we have tacitly assumed that the number of active sites is constant and that there is no initiation period with the prereduced catalyst.

When the reaction is severely diffusion controlled, the rate of polymerization expression must contain the transport information as well as the specific site activity. The rate expression with severe diffusion control is given by eq 11. In this case, insertion time will depend on the one-half power of the active site population. This result was also derived earlier by Chien:[49]

$$R_p = \frac{(k_{rxn}K_AD_{eff})^{1/2}}{R}\alpha[M] \tag{11}$$

Evaluation of kinetics using chromatography is complex; however, the experiment itself is a very simple extension of SGC. Three areas were studied: the initiation period or first exposure of the active catalytic surface to monomer, the influence of temperature on the estimated rate and equilibrium constants, and the influence of quantitative oxygen poisoning on the activity.

Figure 8 shows the development of the elution curves with the number of monomer injections. The amount of monomer per injection is roughly 160 μmol; the number of active chromium atoms in the column is approximately 200 μmol. The first injections resulted in nearly 99% consumption of monomer. The eluting peaks were symmetric in shape, and the retention time was very short, indicating weak surface interaction of the eluted monomer. There is no monomer desorption because the sites initially have no monomer sorbed on the surface. Subsequent injections produce a bimodal peak, a large adsorption–desorption peak accompanied by a smaller symmetric peak. Eventually the symmetric peak disappears, and a single adsorption–desorption peak is found. Many more injections merely replicate this peak; thus we find that accumulation of polymer has no apparent influence on the intrinsic site kinetics. The only influence of polymer accumulation on the surface is in decreasing the monomer diffusivity.

The peak splitting is a transient phenomenon associated with irreversible adsorption and storage of monomer on the surface. Since the zeroth moment increases with exposure to monomer, the monomer consumption rate process decreases. This process may be irreversible adsorption or site insertion. In contrast, the surface adsorption rate process becomes activated by exposure to monomer, resulting in increasing retention of monomer. It is interesting that this same peak splitting is found with ethane adsorption at 50 °C over the same active catalyst (Figure 9). In this case, the fraction of noninteracting ethane is decreased with increasing surface exposure to ethane. This suggests that the ethane adsorption process over active chromium oxide is also activated by surface exposure to solute.

Evaluation of kinetic parameters with the Suzuki–Smith model is a straightforward task. Estimation of the adsorption rate constant requires a difference calculation between the measured second moment and measured intraparticle diffusion time. Accurate measures of the second moment of this type of elution curve were not possible, mainly because of the small elution peak. Even more significant is that accurate values of intraparticle diffusivity are not possible. This problem is further exacerbated by apparently very fast adsorption (the adsorption time constant is very small relative to the measureable diffusion time).

It was possible to determine adsorption rate constants only on the freshly activated and completely poisoned

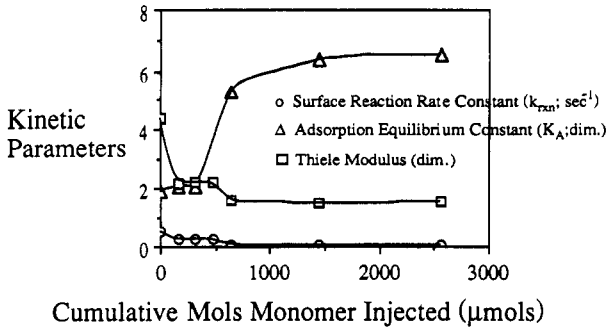

Figure 10. Estimated kinetic parameters during transient initiation.

catalyst. Adsorption is the major rate process in both these situations. For the fresh catalyst the adsorption rate constant was found to be very large, approximately 60 s^{-1} (adsorption equilibrium constant of 2.6). On the completely oxidized catalyst (no polymerization activity), the adsorption rate constant was 33 s^{-1} (adsorption equilibrium constant of 1.1). Kershenbaum[36] reports an adsorption rate constant for butane over alumina at 50 °C as roughly 1500 s^{-1}. Schneider and Smith[15] report 188 s^{-1} for adsorption of ethane on silica gel at 50 °C. We conclude that for polymerization catalyst, adsorption is very fast relative to the surface reaction and we can ignore its influence on the kinetics. For calculation of all rate parameters we utilize the more reliable zeroth and first moments only.

Figure 10 shows the estimated rate and equilibrium parameters as they change during the site initiation period. The surface reaction rate constant (k_{rxn}) and Thiele modulus decline significantly, indicating that exposure to monomer causes immediate site deactivation for the irreversible consumption of monomer. Adsorption equilibrium is increasing, indicating that the surface is storing monomer during transient initiation. The ultimate value of adsorption equilibrium constant at 50 °C is 6.5.

Rates of polymerization for heterogeneous polymerizations are normally expressed as grams of polymer/grams of catalyst/second. Insertion time may be calculated from such conventional rate data in the following manner:

$$\tau_{\text{insertion}} = \frac{\alpha[\text{M}]M_0/K}{\text{d}Y/\text{d}t} = \frac{1}{k_p[\text{R}]} = \frac{1}{k_{rxn}K_A} \qquad (12)$$

Naik[7] measured rates of polymerization of ethylene gravimetrically at 0.1 atm and 90 °C in a fluidized bed reactor. From his results, insertion time is calculated as 1.5 s, with an average rate of polymerization of 0.6 mg of polymer/g of catalyst/s. Webb[50] calculated the insertion time, for the same catalyst at 7 atm and 100 °C in a stirred bed reactor as 2.3 s, with a rate of polymerization of 38 mg of polymer/g of catalyst/s. Catalyst concentrations in either bed were approximately 50 g/L. Both these values are consistent with the SGC results, which predict a steady-state surface insertion time of 3.1 s at 50 °C. The polymerization is apparently first order. SGC as an approach to kinetic analysis seems to be consistent with other experimental techniques used to measure the rate of a solid–gas catalytic reaction.

The steady-state value of the Thiele modulus at 50 °C and 1 atm estimated from the Suzuki–Smith model is 1.6 (effectiveness factor is around 50%). This value would suggest some transport influence of the polymerization even at these very low yields and mild conditions. This value will increase at higher yields as polymer fills pores. Unless particle fragmentation occurs, polymerization will eventually occur only at the exterior particle surface. This was the observation in this work and that of Groeneveld.[48]

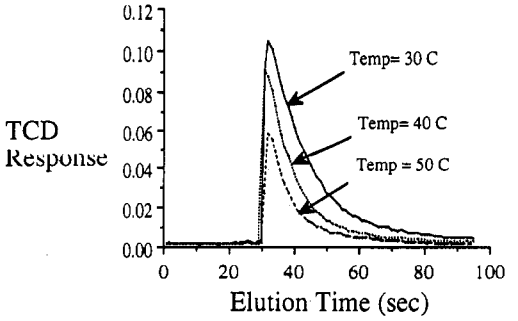

Figure 11. Influence of temperature on the elution of ethylene over active chromium oxide catalyst.

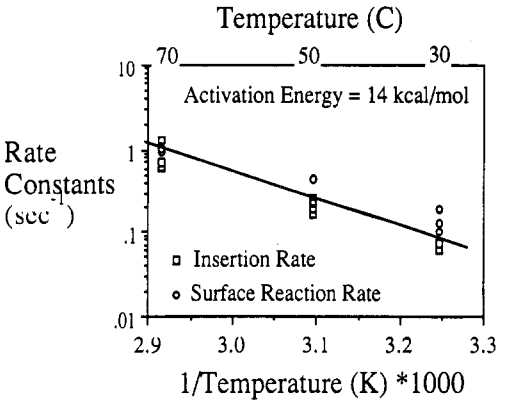

Figure 12. Estimated surface reaction and insertion rate constants at different catalyst temperatures and different number of oxygen-poisoned sites.

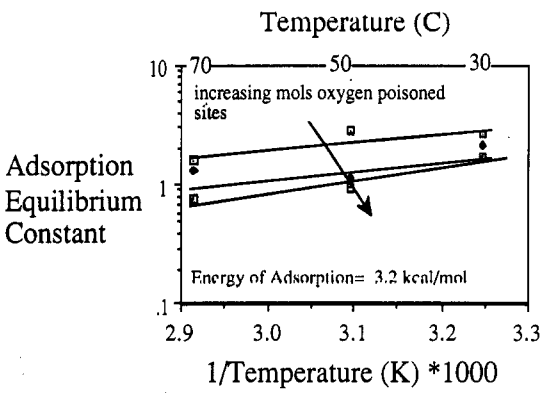

Figure 13. Estimated equilibrium adsorption constant at different catalyst temperatures and different number of oxygen-poisoned sites.

Therefore, monomer transport rate may control the nascent polymerization of ethylene and the morphology of the polymerizing particle.

The influence of temperature on the elution curves is shown in Figure 11. Figures 12 and 13 show the estimated kinetic parameters as a function of temperature and number of oxygen-poisoned sites. The temperature range is quite limited to minimize the complication of changing diffusivity. Also, at higher than 80 °C the activity was so great that monomer elution was not observed. Oxygen may be used as a poison for these sites. The extent of poisoning may be estimated by viewing the progression of the brown discoloration front along the column as oxygen is added to the carrier flow. Oxygen was injected by using the 0.25-cm^3 gas sample loop at a measured pressure and temperature. Column temperature was 50 °C. Oxygen was never found to elute from the column. Oxygen poisoning was done at each temperature to reduce the number of active sites and test for any change in intrinsic activity due to number of sites.

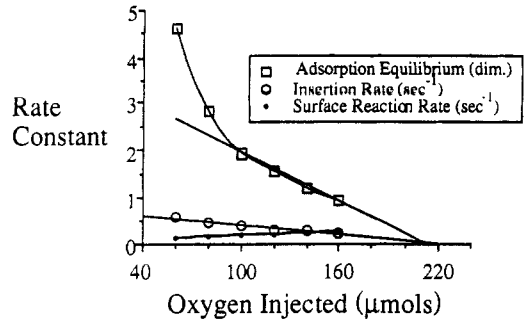

Figure 14. Estimated rate parameters for the remaining active sites at different number of oxygen-poisoned sites.

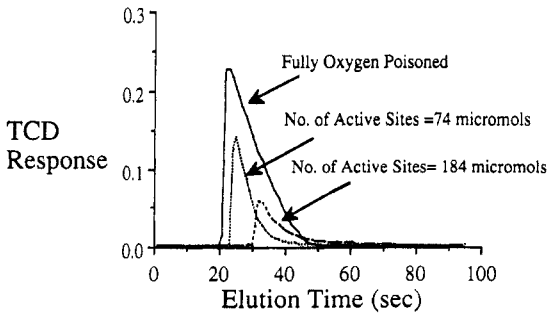

Figure 15. Influence of the number of oxygen-poisoned sites on the elution of ethylene over partially active catalyst.

The apparent activation energy for both the surface reaction and overall insertion rate is around 14 kcal/mol. Both the activation energy and free energy of adsorption are independent of the number of oxygen-poisoned sites. This indicates that oxygen acts as an irreversible, nonselective poison; i.e., it adsorbs on any site independent of its activity. The rather low value is perhaps indicative of the influence of monomer transport on the overall rate of polymerization. The magnitude of these values is consistent with earlier measures by Ayscough,[51] who reported 14.1 kcal/mol between −30 and 0 °C, and Kazanski,[52] who reported 8 kcal/mol with a more active catalyst.

Figure 14 shows the dependence of the various rate constants with the number of active sites. Figure 15 shows some example elution curves of monomer with unpoisoned, partially poisoned, and completely poisoned catalyst. If we linearly extrapolate the insertion rate constant and equilibrium constant to the abscissa, the intercept is an estimate of the number of sites participating in the reaction. This value is roughly 220 μmol, which agrees closely with the calculated number of active chromium atoms in the column. Other site-counting measures that count polymer chains (e.g., tritiated alcohols) predict that only 10–15% of the chromium is actually growing polymer (Karol[11]). We suggest that the number of sites actually making polymer is considerably less than the number of sites participating in sorption of ethylene and oxygen. There may exist two types of chromium sites: one type that is capable of monomer storage and adsorption and another type that is active for insertion and chain growth.

Since the observed insertion time varies linearly with the number of active sites, we can conclude that the rate expression for severe diffusion limitations (eq 11) does not apply for the nascent polymerization at conditions of low pressure and very low yield. This is consistent with the rather low measured Thiele modulus and moderate activation energy. It should be emphasized that this is true only for polymer yields far less than 0.1 g of polymer/g of catalyst. As polymer accumulates, the influence of monomer transport will grow (in the absence of polymerizing particle fragmentation).

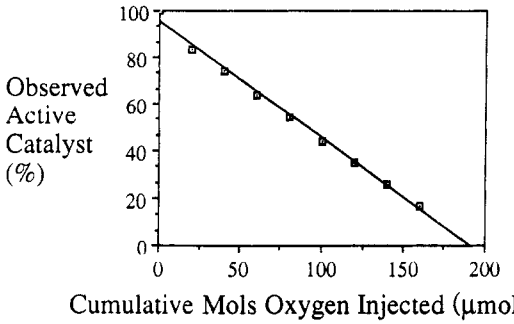

Figure 16. Progression of observable catalyst poisoning with amount of injected oxygen.

The surface reaction rate constant is independent of the number of sites. Thus, the intrinsic activity of the site insertion step does not change with oxygen sorption; only the number of sites is diminished. The overall polymerization rate drops with increased oxygen poisoning because monomer sorption is being blocked by oxygen and not because of some complex site deactivation mechanism.

The adsorption constant decreases initially nonlinearly with oxygen sorption. It is well-known that monomer may be adsorbed on surface sites that are not active for insertion. Apparently, these noninserting sites are more effectively blocked with adsorbed oxygen. For example, one oxygen may block adsorption sites where several ethylenes may adsorb, but the more active polymerization sites may require only one oxygen per site. A linear extrapolation of the equilibrium constant produces an intercept that is the same as that of the site insertion rate constant. Thus, at very low site populations, the number of active sites participating in both adsorption and insertion steps becomes similar.

Figure 16 shows the decrease in observed activity, based on the progression of the brown discoloration of the catalyst in the column, with the cumulative amount of injected oxygen. The decrease in observed activity, by this rather crude method, with moles of oxygen injected, indicates that oxygen removes active insertion and adsorption sites in a constant molar ratio. The abscissa intercept is another indication of number of oxygen adsorbable sites in the column. This value is again close to the calculated amount of active chromium in the column.

Conclusions

Solid–Gas Chromatography as an Analytical Tool. The use of SGC for both kinetics and transport measurements simultaneously is a good way to study isothermal kinetics of catalysts and the influence of pore diffusion. It is, however, complicated, and great care and consideration must be taken to ensure reproducible and reliable results.

Accuracy is compromised somewhat by the unavoidable system influences on the pulse elution dynamics. We feel that the measurement of adsorption rate constants is not reliable with this technique since it relies on a difference calculation between two uncertain measurements, the solute diffusivity and elution curve second moment. This is especially true for situations with fast adsorption processes.

The sensitivity to solute concentration, column pressure drop, and the unsteady nature of SGC limits its accuracy considerably. Properties predicted from a dynamic technique such as SGC may not correspond to those predicted by other methods. Observations from SGC are applicable to the conditions and time scale of the particular experiment. SGC explores mainly macroporosity and is not well-suited as a pore size characterization tool for high-

porosity solids. The technique does measure the important aspects of dynamic transport of solute through a porous particle. Provided the time scales of the reaction process, intraparticle transport process, and elution curve are of similar magnitude, SGC is suited to evaluate Thiele moduli.

Precision and repeatability of SGC with a single-column packing is excellent; thus it is best employed for sensitivity studies, such as poisoning and internal morphological alterations. Careful accounting of system influences and pressure drop, as well proper identification of the major rate process time constants, is essential to good design of the experiment.

Ethylene Polymerization Kinetics over Supported Chromium Oxide Catalyst. Activation has little net influence on the solute transport rate and accessible void space of the polymerization catalyst. Calcination results in sintering and pore collapse with a void space decrease and a reduction of solute diffusivity. Reduction, however, produces an apparent increase in diffusivity and porosity.

Effective diffusivity for these catalysts is very small, around 2×10^{-4} cm^2/s. Such low values cannot be explained by conventional effective medium theory as predicted tortuosities are much too high to be credible. Note that tortuosity estimates are based on an assumption of a uniform void structure and not the bimodal, interconnected network found with these catalysts.

First exposure of active catalyst to monomer is marked by a transient period in which monomer is being irreversibly adsorbed onto the surface. The rate of adsorption is very fast and is not rate limiting. Intrinsic site kinetics are highly sensitive to the accumulation of monomer on the surface during this period.

Once the transient initiation is passed, intrinsic site kinetics are unaffected by the accumulation of polymer. Accumulation of polymer to yields of less than 0.1 g of polymer/g of catalyst does have an influence on the changing polymerizing particle morphology and monomer diffusion resistance. Polymer fills the catalyst macropores, resulting in a decreasing monomer diffusivity. If fragmentation does not occur, polymerization is eventually restricted to the volume nearest the exterior surface where interparticle fusion can cause agglomeration and possibly a decreasing rate of polymerization.

The overall polymerization reaction is controlled by the surface insertion step. Insertion time (τ_{insert}) at 50 °C and 1–2 atm of monomer pressure is around 3.1 s, which is consistent with gravimetric measures for this catalyst. The equilibrium adsorption constant (K_A) at these conditions is 6.5. The surface insertion rate constant (k_{rxn}) is approximately 0.06 s^{-1}.

Thiele modulus for ethylene polymerization at 50 °C in a dilute pulse reactor at atmospheric pressure is around 1.5. This indicates that even at these very mild conditions diffusion limitations may be significant. However, the linearity of the observed activity with number of active sites would argue against severe diffusion limitations. At industrial conditions of high monomer partial pressure, diffusivity will be even lower and the influence of monomer transport on the nascent kinetics may become more significant. In this situation, polymerization and fracture processes will undoubtedly occur from the outside of the macroparticle toward the particle center.

Oxygen poisons the chromium sites in a constant molar ratio. The decrease in polymerization rate with decreasing number of active sites is not due to intrinsic site deactivation. Rate declines due to the decrease in the amount of adsorbed monomer on the surface.

Acknowledgment. We thank the National Science Foundation, Grant 85-15479, the Phillips Petroleum Co. for supplying us with the catalysts, and the Union Carbide Corp. for financial assistance in this work.

Notation

D_{eff}	effective, gas phase, intraparticle diffusion coefficient (cm^2/s)
D_L	axial extraparticle diffusion coefficient (cm^2/s)
K	grams of active catalyst/liter solids bed
K_A	adsorption equilibrium constant (dim)
k_{ads}	adsorption rate constant (s^{-1})
k_p	propagation coefficient (L of solids bed/mol of site/s)
k_{rxn}	surface reaction rate constant (s^{-1}) describing the rate of adsorbed monomer insertion
$k_{rxn}K_A$	insertion rate constant (s^{-1}) describing the rate of gas-phase monomer insertion
L	column length (cm)
M_0	molecular weight of monomer (g/mole of monomer)
[M]	monomer concentration (mol of monomer/L of gas phase)
R	polymerizing particle diameter (cm)
[R]	active site concentration (mol of site/L of solids bed)
R_p	rate of polymerization (mol of monomer/L of solids bed/s)
s^2	variance of elution peak (s^2)
t	time (s)
v_∞	carrier velocity based on tube diameter (cm/s)
Y	polymer yield (g of polymer/g of catalyst)

Greek Characters

α	extraparticle void space = volume of gas phase/volume solids bed (dim)
β	intraparticle void space = accessible void space of particle/total particle volume (dim)
$\tau_{insertion}$	time constant for insertion of gas-phase monomer
μ_1	mean retention time of elution peak (s)
ϕ^2	Thiele modulus (eq 5)

Registry No. Ethylene, 74-85-1; chromium oxide, 11118-57-3.

References and Notes

(1) Chiovetta, M. G.; Laurence, R. L. Heat and Mass Transfer During Polymerization of α-Olefins from the Gas Phase. Paper presented at the Berlin Workshop on Polymer Reaction Engineering, 1983.
(2) Choi, K. Y.; Ray, W. H. Recent Developments in Transition Metal Catalyzed Olefin Polymerization. *J. Macromol. Sci. Rev. Macromol. Chem. Phys.* **1985**, *C25*(4), 1–91.
(3) Floyd, S.; Choi, K. Y.; Taylor, T. W.; Ray, W. H. Polymerization of Olefins through Heterogeneous Catalysis III: Polymer Particle Modeling with an Analysis of Intraparticle Heat and Mass Transfer Effects. *J. Appl. Polym. Sci.* **1986**, *32*, 2935–2960.
(4) Ray, W. H. Practical Benefits of Modelling Olefin Polymerization Reactions. Presented at the International Symposium on Transition Metal Catalyzed Polymerizations. University of Akron, June, 1986.
(5) Weist, E. L.; Ali, A. H.; Conner, W. C. Morphological Study of Supported Chromium Oxide Polymerization Catalysts I Activation. *Macromolecules* **1987**, *20*, 689–693.
(6) Ali, A. Kinetics and Morphology Study of Phillips Polymerization Catalyst, Masters Thesis, Department of Chemical Engineering, University of Massachusetts, Amherst, 1985.
(7) Naik, B. Characterization of Polyethylene Produced at Low Yield via Supported Chromium Oxide Catalysts. Masters Thesis, Department of Chemical Engineering, University of Massachusetts, 1987.
(8) Weist, E. L. Morphological Study of Silica-Supported Chromium Catalysts for Ethylene Polymerization. Ph.D. Thesis, Department of Chemical Engineering, University of Massachusetts, Amherst, 1988.
(9) McDaniel, M. P. Fracturing Silica Based Catalysts During Ethylene Polymerization. *J. Polym. Sci., Polym. Chem. Ed.* **1981**, *19*, 1967–1976.
(10) McDaniel, M. P. Controlling Polymer Properties with the Phillips Chromium Catalyst. *Ind. Eng. Chem. Res.* **1988**, *27*, 1559–1564.
(11) Karol, F. J. Studies of High Activity Catalysts for Olefin Polymerization. *Catal. Rev. Sci. Eng.* **1984**, *26*, 557–583.

(12) Munoz-Escalona, A.; Hernandez, G.; Gallardo, J. A. Catalytic Activity and Control of the Nascent Morphology of Polyethylene Obtained with First and Second Generation Ziegler-Natta Catalysts. *J. Appl. Polym. Sci.* **1984**, *29*, 1887–1282.
(13) Kubin, M. Beitrag zur Theorie der Chromatographie. *Collect. Czech. Chem. Commun.* **1965**, *30*, 1105–1116.
(14) Kucera, E. Contribution to the Theory of Chromatography: Linear, Non-Equilibrium Elution Chromatography. *J. Chromatogr.* **1965**, *19*, 237–248.
(15) Suzuki, M.; Smith, J. M. Kinetic Studies by Chromatography. *Chem. Eng. Sci.* **1971**, *26*, 221–235.
(16) Conder, J. L.; Young, C. L. Physicochemical Measurements by Gas Chromatography; Wiley: New York, 1979.
(17) Furasawa, T.; Suzuki, M.; Smith, J. M. Rate Parameters in Heterogeneous Catalysis by Pulse Testing. *Catal. Rev.-Sci. Eng.* **1976**, *13*(1), 43–74.
(18) Sagara, M.; Schneider, P.; Smith, J. M. The Determination of Heat Transfer Parameters for Flow in Packed Beds using Pulse Testing and Chromatography Theory. *Chem. Eng. J.* **1970**, *1*, 47–56.
(19) Suzuki, M.; Smith, J. M. Chemisorption Rates by Chromatography: Hydrogen on Copper-Zinc Oxide. *J. Catal.* **1971**, *21*, 336–348.
(20) Padberg, G.; Smith, J. M. Chemisorption Rates by Chromatography. *J. Catal.* **1968**, *12*, 172–182.
(21) Schneider, P.; Smith, J. M. Adsorption Rate Constants from Chromatography. *AIChE J.* **1968**, *14*(5), 763–771.
(22) Chui, H. M.; Hashimoto, N.; Smith, J. M. Chromatographic Studies of Adsorption of Nitric Oxide on Activated Carbon. *Ind. Eng. Chem. Fundam.* **1974**, *13*(3), 282–285.
(23) Galan, M. A.; Suzuki, M.; Smith, J. M. Effect of Adsorption Characteristics on Pulse Retention Times. *Ind. Eng. Chem. Fundam.* **1975**, *14*(3), 274–275.
(24) Cerro, R. L.; Smith, J. M. Effects of Heat Release and Non-Linear Equilibrium on Transient Adsorption. *Ind. Eng. Chem. Fundam.* **1969**, *8*(4), 797–802.
(25) Edwards, M. F.; Richardson, J. F. Gas Dispersion in Packed Beds. *Chem. Eng. Sci.* **1968**, *23*, 109–123.
(26) Schanel, L.; Schneider, P. Axial Dispersion due to Molecular Diffusion in Gas Chromatography. *Chem. Eng. J.* **1971**, *2*, 274–278.
(27) Scott, D. S.; Lee, W.; Papa, J. The Measurement of Transport Coefficients in Gas-Solid Heterogeneous Reactions. *Chem. Eng. Sci.* **1968**, *29*, 2155–2167.
(28) Baiker, A.; New, M.; Richarz, W. Determination of Intraparticle Diffusion Coefficients in Catalyst Pellets: A Comparative Study of Measuring Methods. *Chem. Eng. Sci.* **1982**, *32*, 643–656.
(29) Cerro, R. L.; Smith, J. M. Chromatography of Non-Adsorbable Gases. *AIChE J.* **1970**, *16*(6), 1034–1040.
(30) Sarma, P. N.; Haynes, H. W. GC for Diffusion in Zeolites. *Adv. Chem. Ser.* **1974**, *No. 133*, 205–217.
(31) Schneider, P.; Smith, J. M. Chromatography Study of Surface Diffusion. *AIChE J.* **1968**, *14*(6), 887–894.
(32) Nir, A.; Pismen, L. M. Simultaneous Intraparticle Forced Convection, Diffusion and Reaction in a Porous Catalyst. *Chem. Eng. Sci.* **1977**, *32*, 35–41.
(33) Rodrigues, A. L.; Ahn, B. J.; Zoulalian, A. Intraparticle Forced Convection Effects in Catalyst Diffusion Measurements and Reactor Design. *AIChE J.* **1982**, *28*(4), 541–546.
(34) Dixon, A. G.; Ma, Y. H. A Comparison of Moment Methods for Non-isobaric Gas Chromatography Columns. *Chem. Eng. Sci.* **1988**, *43*(6), 1297–1302.
(35) Carleton, F. B.; Kershenbaum, L. S.; Wakeham, W. A. Adsorption in Non-isobaric Fixed Beds. *Chem. Eng. Sci.* **1978**, *33*, 1239–1246.
(36) Kershenbaum, L. S.; Kohler, M. A. Adsorption in Non-isobaric Fixed Beds: Measurement of Rates of Adsorption. *Chem. Eng. Sci.* **1984**, *39*(4), 1423–1426.
(37) Schneider, P.; Gelbin, D. Direct Transport Parameter Measurement versus Their Estimation from Mercury Penetration in Porous Solids. *Chem. Eng. Sci.* **1985**, *40*(7), 1093–1099.
(38) Foth, P.; Petrini, G.; Schneider, P. Transport Parameters of Monodisperse Porous Catalysts. *Coll. Czech. Chem. Commun.* **1983**, *48*, 215–227.
(39) Miller, G. A.; Bailey, J. E. Some New Results for Chromatography Kinetic Studies. *AIChE J.* **1973**, *19*(4), 876–882.
(40) Schneider, P. Determination of Effective Diffusion Coefficients for Porous Packings with an Impermeable Centre from Peak Moments. *Chem. Eng. Sci.* **1986**, *41*(7), 1759–1764.
(41) Gangwal, S. K.; Hudgins, R. R.; Brydsen, A. W.; Silveston, P. L. Interpretation of Chromatographic Peaks by Fourier Analysis. *Can. J. Chem. Eng.* **1971**, *49*, 113–119.
(42) Pawlisch, C. A.; Bric, J. B.; Laurence, R. L. Solute Diffusion in Polymers: Fourier Estimation of Capillary Column Inverse Gas Chromatography Data. *Macromolecules* **1985**, *21*, 1685–1698.
(43) Kokes, R. J.; Tobin, H.; Emmett, P. H. A New Microcatalytic-Chromatographic Technique for Study of Catalytic Reactions. *J. Am. Chem. Soc.* **1955**, *77*, 5860.
(44) Gaziev, G. A.; Filinoskii, V. Y.; Yanuskii, M. I. Kinetics of Heterogeneous Catalytic Reactions in Chromatographic Pulses under Conditions of Ideal Linear Chromatography. *Kinet. Catal. (Engl. Transl.)* **1963**, *4*, 599–608.
(45) Blanton, W. A.; Byers, C. H.; Merrill, R. P. Quantitative Rate Coefficients from Pulsed Microcatalytic Reactors. *Ind. Eng. Chem. Fundam.* **1968**, *7*(4), 611–621.
(46) Wethorold, R. G.; Wissler, E. H.; Bischoff, K. B. An Experimental and Computational Study of the Hydrolysis of Methyl formate in a Chromatographic Reactor. *Adv. Chem. Ser.* **1974**, *No. 133*, 181–190.
(47) Cho, B. K.; Carr, R. W.; Aris, R. A Continuous Chromatographic Reactor. *Chem. Eng. Sci.* **1980**, *35*, 74–81.
(48) Groeneveld, C.; Wittgen, P.; Lavrijsen, J.; Schuit, G. Hydrogenolysis and Polymerization of Ethylene over Chromium Oxide-Silica Catalyst. *J. Catal.* **1983**, *82*, 77–91.
(49) Chien, J. C. W. Criteria for Diffusion Limitation in Coordination Polymerization. *J. Polym. Sci., Polym. Chem. Ed.* **1979**, *17*, 2555–2565.
(50) Webb, S. W.; Conner, W. C.; Laurence, R. L. Department of Chemical Engineering, University of Massachusetts, Amherst, MA, 1988, unpublished data.
(51) Ayscough, P. B.; Eden, C.; Steiner, H. The Polymerization of Ethylene over Supported Chromium Oxide. *J. Catal.* **1965**, *4*, 278–290.
(52) Kazanski, V. B.; Turkevich, H. Kinetics and ESR Studies of Ethylene Polymerization on Chromia-Silica Catalyst. *J. Catal.* **1967**, *8*, 231–239.